NUCLEAR STRUCTURE THEORY OF THE HEAVIEST NUCLEI*

A.V. Afanasjev, S.E. Agbemava

Department of Physics and Astronomy, Mississippi State University
P.O. Drawer 5167, Mississippi State, MS 39762-5167, USA

(Received January 29, 2015)

The current status of the application of covariant density functional theory to the description of actinides and superheavy nuclei is reviewed. The achievements and open problems are discussed.

DOI:10.5506/APhysPolB.46.405
PACS numbers: 21.10.Dr, 21.10.Pc, 21.60.Jz, 23.60.+e

1. Introduction

There is a considerable activity (both in theory and experiment) in the study of shell-stabilized superheavy nuclei (SHN) [1, 2]. These studies are characterized by a number of experimental and theoretical challenges. The experimental challenges are the results of the experiments with low production cross sections and analyses based only on few events. The theoretical challenges are, in part, the consequences of different predictions for the centers of the island of stability of SHN. Macroscopic+microscopic (MM) method, non-relativistic density functional theories (DFT) and covariant DFT (further CDFT [3]) predict these centers at different proton and neutron numbers. For example, these islands are predominantly centered at ($Z = 114, N = 184$) and ($Z = 126, N = 184$) in the MM and Skyrme DFT, respectively [1, 4]. On the contrary, covariant energy density functionals (CEDFs) predict large shell gap at $Z = 120$; however, neutron gap can be localized either at $N = 172$ (in most of the cases) and/or at $N = 184$ [4–6]. In this situation, it is important to understand the sources of the differences and uncertainties in the prediction of the shell structure of SHN and how they affect the physical observables (deformations, fission and α-decay observables) of interest. The actinides (the heaviest nuclei for which

* Presented at the Zakopane Conference on Nuclear Physics "Extremes of the Nuclear Landscape", Zakopane, Poland, August 31–September 7, 2014.

detailed spectroscopic and fission information exists) play here a role of testing ground for the state-of-the-art nuclear structure models. We focus here on the results obtained with CDFT during last five years.

2. Single-particle structure

The presence of the island of stability of SHN is due to large shell gaps in the single-particle spectra. The neutron and proton single-particle spectra obtained in spherical relativistic mean field (RMF) calculations of the $^{292}120$ and $^{304}120$ nuclei are shown in Fig. 1[1]. In order to create a more representative statistical ensemble, the calculations have been performed with 10 CEDFs. Amongst those are the CEDFs NL3*, DD-ME2, DD-MEδ and

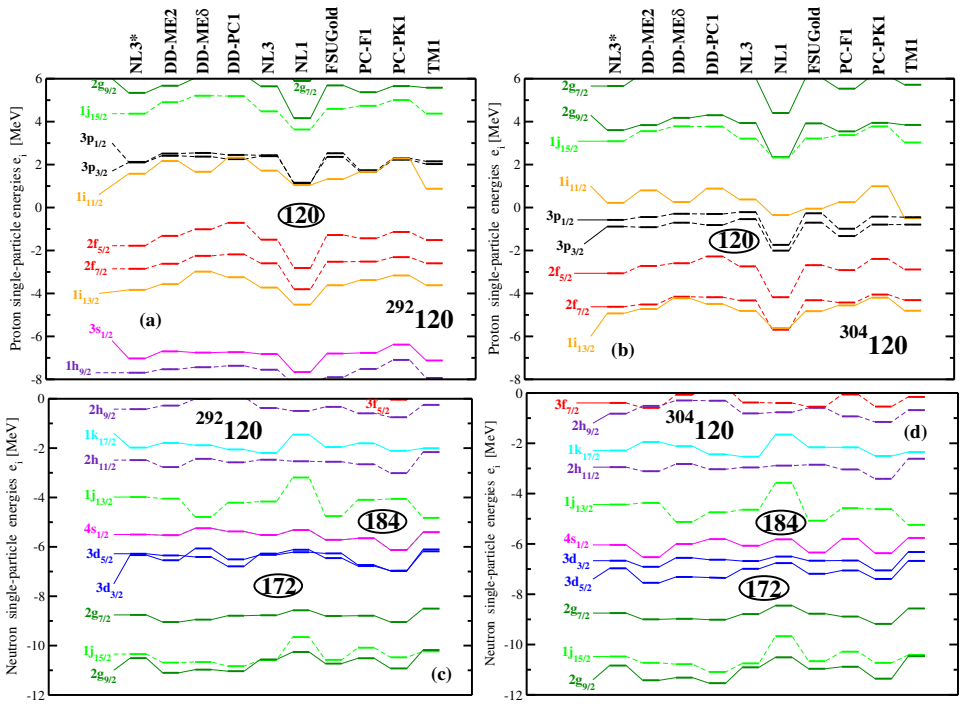

Fig. 1. Neutron (left panels) and proton (right panels) single-particle states at spherical shape in the $^{292}120$ and $^{304}120$ SHN. They are determined with the indicated CEDFs in the RMF calculations without pairing. Solid and dashed connecting lines are used for positive and negative parity states. Spherical gaps are indicated; all the states below these gaps are occupied in the ground state configurations.

[1] Similar figures are presented for some other CEDFs in Refs. [5, 6]. Reference [5] also provides detailed comparison with non-relativistic Skyrme DFT results.

DD-PC1, the global performance of which has been studied in Ref. [7]. One can see that the $Z = 120$ and $N = 172$ shell gaps are especially pronounced in the $^{292}120$ nucleus. This is a consequence of the presence of central depression in density distribution generated by a predominant occupation of the high-j orbitals above the ^{208}Pb nucleus [8]. The increase of neutron number from $N = 172$ up to $N = 184$ is associated with the occupation of low-j neutron orbitals which leads to a flatter density distribution in the $N = 184$ system [8]. As a consequence, the $Z = 120$ and $N = 184$ shell gaps are reduced and $N = 184$ gap is increased. As one can see in Fig. 1, these are rather general features which are independent of the CEDF.

Figure 1 clearly shows that there are theoretical uncertainties in the description of the energies of the single-particle states, their relative positions and the size of large shell gaps. The latter is summarized in Fig. 2, which shows the average sizes of these gaps and the spreads in their predictions. In addition, these gaps in SHN are also compared with the calculated gaps in the nuclei ^{56}Ni, ^{100}Sn, ^{132}Sn and ^{208}Pb. The general trend of the decrease of the size of the shell gaps with proton and neutron numbers are clearly visible. Definitely, the impact of theoretical uncertainties (shown by the spread of the sizes of the calculated gaps in Fig. 2) on model predictions depends on relative sizes of theoretical uncertainties and calculated shell gaps.

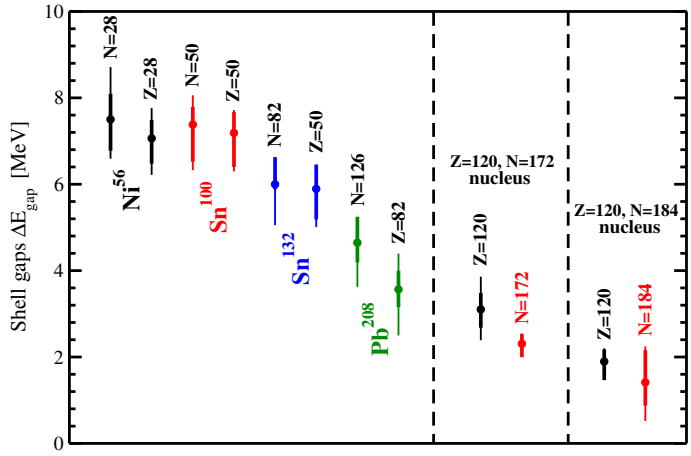

Fig. 2. Neutron and proton shell gaps $\Delta E_{\rm gap}$ of the indicated nuclei. The average (among ten used CEDFs) size of the shell gap is shown by a solid circle. Thin and thick vertical lines are used to show the spread of the sizes of the calculated shell gaps; the top and bottom of these lines correspond to the largest and smallest shell gaps amongst the considered set of CEDFs. Thin lines show this spread for all employed CEDFs, while thick lines are used for the subset of four CEDFs (NL3*, DD-ME2, DD-MEδ and DD-PC1). Particle numbers corresponding to the shell gaps are indicated.

The presence of theoretical uncertainties has less severe consequences on the predictions of magic nuclei in $A \leq 208$ nuclei than on similar predictions for SHN.

The present analysis strongly suggests that in order to make reliable predictions for SHN one needs a high predictive power for the energies of the single-particle states. It is also clear from Figs. 1 and 2 that the improvement in the DFT description of the energies of the single-particle states in known nuclei will also reduce the uncertainties in the prediction of the shell structure of SHN. Unfortunately, the detailed investigation of the single-particle degrees of freedom in the CDFT framework is in an initial stage. This is because the coupling of the single-particle motion with vibrations has to be taken into account (especially in spherical nuclei). So far, the accuracy of the description of the energies of the single-particle states and the sizes of shell gap in spherical nuclei has been studied in relativistic particle-vibration [9] and quasiparticle-vibration [10] coupling models with the CEDF NL3* [11] only. The experimentally known gaps of ^{56}Ni, ^{132}Sn and ^{208}Pb are reasonably well described in the relativistic particle-vibration calculations of Ref. [9]. The impact of particle vibration on spherical shell gaps in SHN has been investigated in Refs. [9, 12]. Although particle-vibration coupling decreases the size of shell gaps, the $Z = 120$ gap still remains reasonably large but there is a competition between smaller $N = 172$ and $N = 184$ gaps. The accuracy of the description of the energies of one-quasiparticle deformed states in the rare-earth region and actinides has been statistically evaluated in Ref. [13] within the framework of relativistic Hartree–Bogoliubov theory. On the one hand, these studies have proved a success of CDFT; the covariant functionals provide a reasonable description of the single-particle properties despite the fact that such observables were not used in their fit. On the other hand, they illustrate the need for a better description of the single-particle energies.

3. The α-decay properties and the deformations of the ground states

In the superheavy nuclei, spontaneous fission and α emission compete and shortest half-live determines the dominant decay channel and the total half-live. Only in the case when spontaneous fission half-live of the nucleus is longer than half-live of α emission then superheavy nuclei can be observed in experiment. In addition, only nuclei with half-lives longer than $\tau = 10$ μs are observed in experiments.

The α decay half-live depends on the Q_α values. The Q_α values, obtained in the RHB calculations with the DD-PC1 [15] and NL3* [11] CEDFs, are compared with experimental ones in Fig. 3. One can see that reasonable

agreement with experimental data is achieved in both calculations. However, on average, somewhat better description is obtained with DD-PC1 CEDF. This is a consequence of different fitting protocols[2] and the fact that the binding energies are better described in DD-PC1 [7].

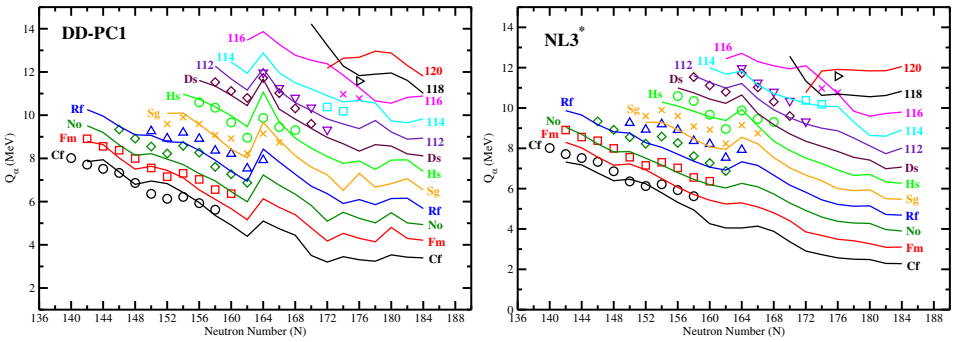

Fig. 3. Q_α values of even–even superheavy elements as predicted by the RHB calculations with indicated CEDFs. The formalism of Ref. [7] is used in the RHB calculations. Experimental Q_α values are extracted from experimental masses of Ref. [14].

The presence of the deformed $N = 162$ shell gap reveals itself in the presence of the peak at $N = 164$ in the Q_α curves at fixed proton number. The magnitude of this peak is dependent on the $N = 162$ shell gap. This peak is seen in experimental data of the Rf, Sg, Hs and Ds isotopic chains. On average, the magnitude of this peak is somewhat underestimated (overestimated) in the NL3* (DD-PC1) CEDF.

The comparison of experimental data with the calculated Q_α curves obtained in the CDFT (Fig. 3 in the present manuscript and Fig. 18 in Ref. [16]) and the ones obtained in non-relativistic models (see, for example, Fig. 18 in Ref. [16] and Figs. 44 and 45 in Ref. [1]) clearly indicate that available experimental data does not allow to distinguish the predictions of different models in respect of the position of the center of the island of stability.

The calculated charge quadrupole deformations for these two CEDFs are plotted in Fig. 4. They reveal some interesting features which have not been discussed before. The $Z = 120$ and $N = 184$ SHN are spherical in the NL3* CEDF. On the contrary, the $Z = 120, N \geq 174$ nuclei are oblate in the ground state in the DD-PC1 CEDF. This is in contradiction with the expectations (based on large size of the $Z = 120$ gap (Fig. 1)) that the $Z = 120$ chain has to be spherical in the ground states in both CEDFs. This

[2] The DD-PC1 CEDF has been fitted to 64 deformed nuclei in the rare-earth region and actinides and NL3* to only 12 spherical nuclei (see Sect. II of Ref. [7] for a detailed comparison of these two CEDFs).

result clearly indicates that the softness of potential energy surface has to be taken into account when analyzing shell structure of SHN. Unfortunately, this fact is neglected in the analysis of shell structure of superheavy nuclei by means of the so-called "two-nucleon shell gap" in Refs. [6, 17] which is performed using the results of spherical calculations.

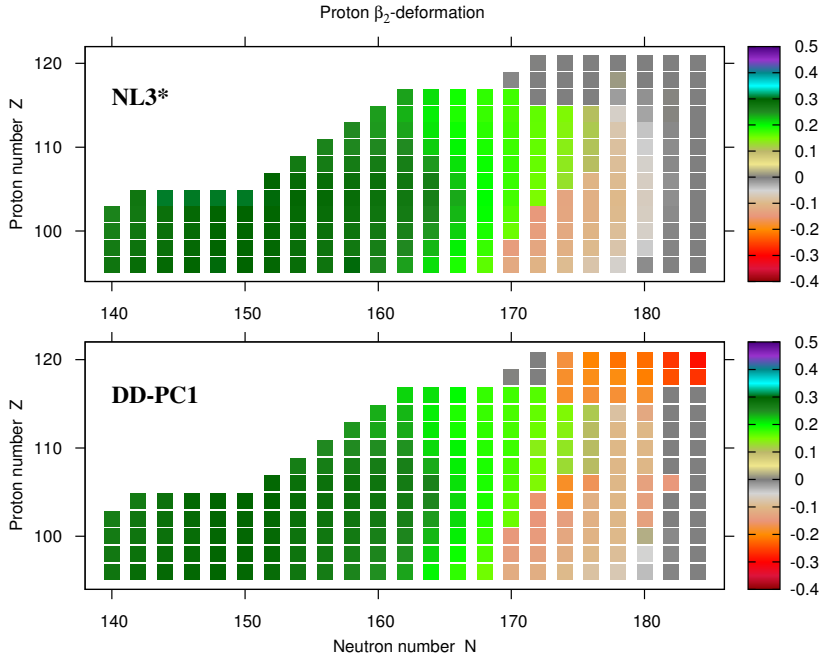

Fig. 4. Charge quadrupole deformations β_2 obtained in the RHB calculations with indicated CEDFs.

4. Fission barriers in superheavy nuclei

The properties of fission barriers is another important quantity which defines the stability of SHN. The systematic investigation of fission barriers in superheavy nuclei has been performed in the RMF+BCS framework with the NL3* CEDF in Ref. [18]. The presence of a doubly-humped fission barrier structure in SHN is an example of the most striking difference between the relativistic and non-relativistic calculations; no outer fission barrier appears in absolute majority of non-relativistic calculations in the $Z \geq 110$ SHN. The inclusion of triaxiality or octupole deformation in the RMF+BCS calculations always lowers (by around 2 MeV in the majority of the nuclei) the outer fission barrier as compared with the results of axially symmetric calculations. The underlying shell structure clearly defines which

of the outer fission barrier saddle points (triaxial or octupole deformed) is lower in energy. For example, the lowest saddle point is obtained in triaxial calculations in proton-rich nuclei with $N < 174$ (Ref. [18]). On the contrary, the lowest saddle point is obtained in octupole deformed calculations in neutron-rich nuclei with $N > 174$.

Figure 5 shows how the models which have been benchmarked in a systematic way in the actinides extrapolate to the region of superheavy nuclei. These models describe inner fission barriers of actinides very accurately (see Fig. 2 in Ref. [18] and Ref. [19]). However, their predictions for SHN vary wildly; the difference in inner fission barrier heights between different models reaches 6 MeV in some nuclei. The more surprising fact is that the prediction of two macroscopic+microscopic (MM) models differs so substantially. As discussed in Ref. [18], very limited experimental data on fission barriers in SHN is not reliable enough to distinquish between these model predictions.

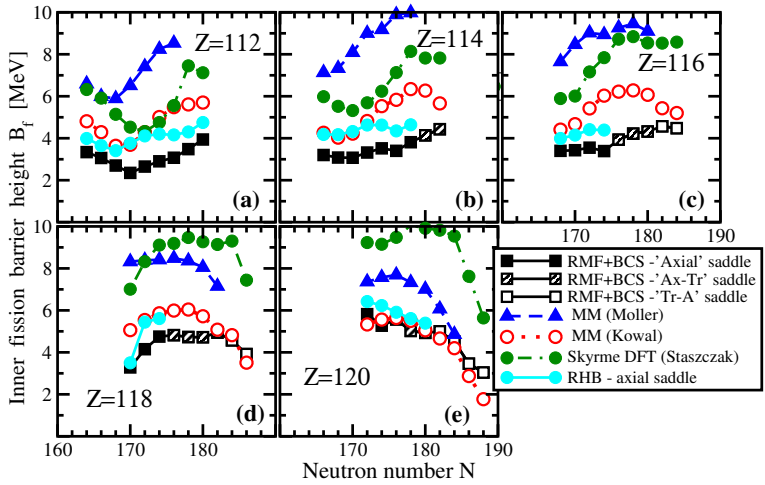

Fig. 5. Inner fission barrier heights B_f as a function of neutron number N. The results of the MM calculations are taken from Ref. [26] (labeled as 'MM (Möller)') and Ref. [27] (labeled as 'MM (Kowal)'). The position of inner fission barrier saddle in deformation space varies as a function of particle number. The labeling of Ref. [18] is used in order to indicate whether the saddle is axial (labeled as 'Axial'), has small ($\gamma \sim 10°$, labeled as 'Ax-Tr') or large ($\gamma \sim 25°$, labeled as 'Tr-A') γ-deformations in the RMF+BCS calculations. The results of Skyrme DFT calculations with SkM* EDF have been taken from Ref. [28].

In addition to the RMF+BCS fission barriers, we present also new results of axial RHB calculations (labeled as "RHB-axial saddle"); the latter are restricted to nuclei in which the saddle of inner fission barrier is axial in the RMF+BCS calculations. The principal difference between these two

calculations lies in the treatment of pairing. The monopole pairing is used in the RMF+BCS calculations [18] and its strength is defined by the fit to "empirical" pairing gaps of Ref. [20]. On the contrary, the separable pairing force of finite range is used in the RHB calculations and its pairing strength is defined by the fit to the moments of inertia in the actinides [21]. The differences in calculated inner fission barriers are due to: *(i)* different extrapolation properties of these two types of pairing ongoing from actinides to superheavy region and *(ii)* the dependence of fission barrier heights on the range (zero or finite) of pairing interaction [22]. Because of these reasons, the RHB results for the heights of inner fission barriers are higher than the RMF+BCS ones by roughly 1 MeV. Furthermore, they come closer to the 'MM (Kowal)' model predictions.

Instead of fission barriers (which is indirectly measured quantity), one can consider spontaneous fission half-lives $\tau_{\rm SF}$ which is a directly measured quantity. However, the calculations of spontaneous fission half-lives represents a real challenge. This is because there are significant uncertainties in $\tau_{\rm SF}$ which emerge from different building blocks entering the standard semiclassical Wentzel–Kramers–Brillouin (WKB) formula [23] which is used in the calculations of $\tau_{\rm SF}$. These uncertainties have been analyzed in detail in Refs. [24, 25].

The calculated values of spontaneous fission half-lives also strongly depend on the underlying theory used to describe collective motion (typically the adiabatic time-dependent HFB (ATDHFB) or the generator coordinate method (GCM)) and the approximations involved in the evaluation of the inertias; for a given nucleus, the difference between the $\tau_{\rm SF}$ values calculated with ATDHFB and GCM can reach many orders of magnitude [25]. The $\tau_{\rm SF}$ values also strongly depend on the poorly defined energy E_0 entering into action integral S; again, the uncertainties reach several orders of magnitude.

It was also shown in Ref. [24] that fission pathways strongly depend on assumptions underlying collective inertia. Perturbative cranking approximation, commonly used in ATDHFB, underestimates the variations of mass parameters due to level crossings (configuration changes). As a result, a collective inertia drives dynamical fission path to near-axial shapes. When non-perturbative cranking inertia is employed, strong triaxiality is predicted for dynamical fission path in agreement with static calculations. So far, this result has been obtained only for a single nucleus in Ref. [24] and it remains to be seen whether it is a general conclusion.

Unfortunately, no studies of spontaneous fission half-lives are available in the CDFT so far. This is contrary to the case of non-relativistic DFT's in which extensive studies of spontaneous fission half-lives have been performed (see Refs. [23–25] and reference therein).

5. Rotational excitations in actinides and light superheavy nuclei

Figures 6 and 7 show the results of the first ever (in any DFT framework) systematic investigation of rotational properties of even–even and odd-mass nuclei at normal deformation [21, 30]. The calculations are performed within the CRHB+LN approach [4, 31]. The gradual increases of the moments of inertia below band crossings are reproduced well. Either sharp or more gradual increases of the kinematic moments of inertia calculated at $\Omega_x \approx$ 0.2–0.30 MeV are due to the alignments of the neutron $j_{15/2}$ and proton $i_{13/2}$ orbitals which, in many cases, take place at similar rotational frequencies. The upbendings observed in a number of rotational bands of even–even $A \geq 242$ nuclei are well described in model calculations (see Refs. [21, 30] for details). However, the calculations also predict similar upbendings in lighter nuclei which have not been seen in experiment. The stabilization of

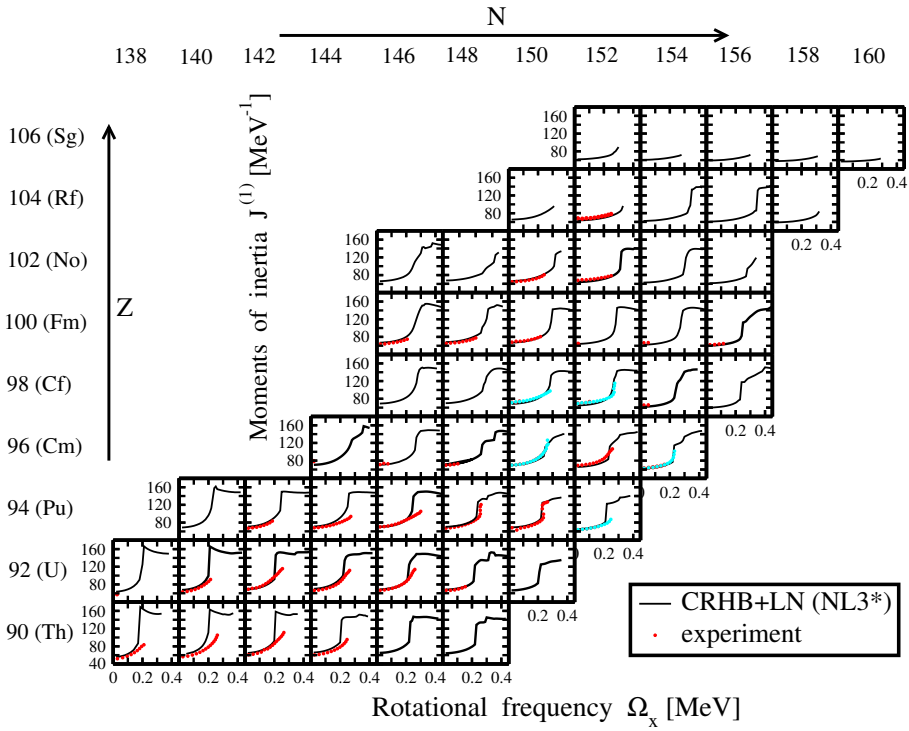

Fig. 6. The experimental and calculated kinematic moments of inertia $J^{(1)}$ as a function of rotational frequency Ω_x. The calculations are performed with the NL3* CEDF [11]. Calculated results and experimental data are shown as black lines and dark gray/red dots, respectively. Light gray/cyan dots show new experimental data from Ref. [29] which were not included in Ref. [21]. From Refs. [21, 30].

octupole deformation at high spin, not included in the present CRHB+LN calculations, could be responsible for this discrepancy between theory and experiment [21].

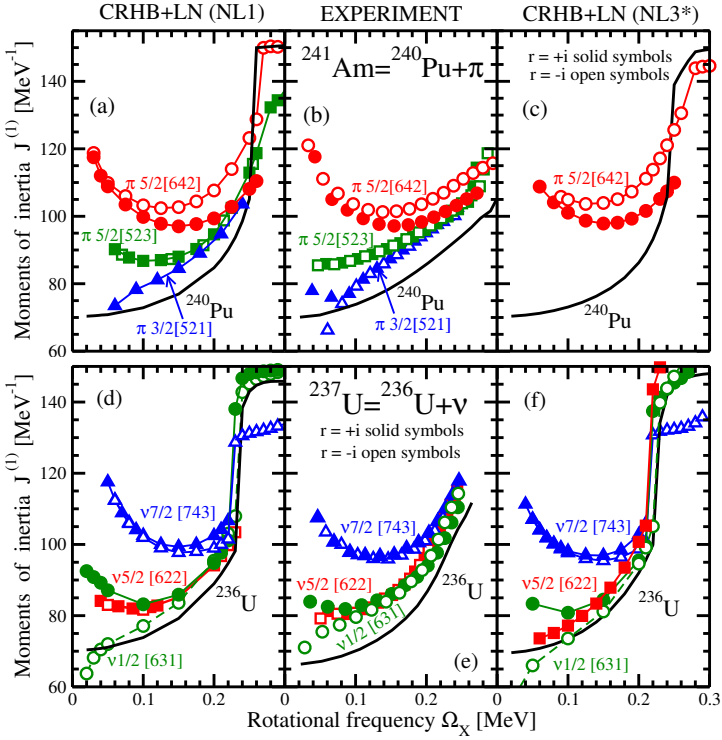

Fig. 7. (Top panels) Calculated and experimental kinematic moments of inertia $J^{(1)}$ of the indicated one-quasiproton configurations in the ^{241}Am nucleus and ground state rotational band in reference even–even ^{240}Pu nucleus. Experimental data are shown in the middle panel, while the results of the CRHB+LN calculations with the NL1 and NL3* CEDFs in the left and right panels, respectively. The same symbols/lines are used for the same theoretical and experimental configurations. The symbols are used only for the configurations in odd-mass nucleus; the ground state rotational band in the reference even–even nucleus is shown as solid black line. The label with the following structure "Odd nucleus = reference even+even nucleus + proton(π)/neutron(ν)" is used to indicate the reference even–even nucleus and the type of the particle (proton or neutron) active in odd-mass nucleus. (Bottom panels) The same as in top panels but for one-quasineutron configurations in ^{237}U and ground state band in ^{236}U. The experimental data are from Refs. [33, 34]. Based on Ref. [21].

The CRHB+LN approach provides much more consistent description of rotational properties in paired regime as compared with the cranked shell model plus particle-number conserving method (CSM+PNC) approach of Ref. [32]. This is because it was necessary to adjust in the CSM+PNC approach the parameters of the Nilsson potential to experimental single-particle energies, use experimental deformations and employ different pairing gaps in even–even and odd-mass nuclei in order to obtain comparable in accuracy with CRHB+LN approach the description of experimental rotational properties of actinides [30].

In the DFT framework, the description of rotational bands in odd-mass nuclei is more technically difficult than the one in even–even nuclei. First, the effects of blocking due to odd particle have to be included in a fully self-consistent way which is done in the CRHB+LN computer code according to Refs. [35, 36]. The blocking requires the identification of blocked orbital at all frequencies of interest and at all iterations which is non-trivial problem [21]. Second, variational calculations with blocked orbital(s) are numerically less stable than the ones for the ground state bands in even–even nuclei because at each iteration of the variational procedure blocked orbital has to be properly identified. In general, the convergence depends on the interaction and relative energies of blocked orbital and its neighbour within a given parity/signature block (see Sect. V of Ref. [21]).

A representative example of the CRHB+LN calculations for one-quasiparticle bands in ^{237}Np and ^{241}Am is shown in Fig. 7; it comes from systematics of Ref. [21]. One can see that theoretical calculations describe well the absolute values of the kinematic moments of inertia of different one-quasiparticle configurations, their evolution with rotational frequency, signature splitting and their relative properties with respect of the reference band in even–even nucleus. With few exceptions this is also true for other bands studied in Ref. [21]. Figure 7 and Ref. [21] also indicate that the results of the CRHB+LN calculations for a specific configuration only weakly depend on CEDF. The dependence of the convergence on the CEDF is clearly seen on the example of the $\pi 5/2[523]$ and $\pi 3/2[521]$ configurations in ^{241}Am for which no convergence (convergence) has been obtained in the NL3* (NL1) CEDF.

The systematic studies of Ref. [21] allowed to conclude that rotational properties of one-quasiparticle configurations substantially depend on the structure of blocked orbital. As a result, these properties reflected through the following fingerprints:

— the presence or absence of signature splitting,

— the relative properties of different configurations with respect of each other and/or with respect to the ground state band in reference even–even nucleus,

— the absolute values of the kinematic moments of inertia (especially at low rotational frequencies) and their evolution with rotational frequency

provide useful tools for quasiparticle configuration assignments. Such configuration assignments are important, for example, for on-going experimental investigations of odd-mass light superheavy nuclei at the edge of the region where spectroscopic studies are still feasible (the nuclei with masses $A \sim 255$ and proton number $Z \geq 102$) [2, 21]. However, it is necessary to recognize that the configuration assignment based on rotational properties has to be complemented by other independent methods and has to rely on sufficient experimental data [21].

6. Conclusions

In conclusion, a short review of the recent progress in the study of actinides and superheavy nuclei within covariant density functional theory has been presented. It also includes new results displayed in Figs. 1–5 which have not been published before. The uncertainties in the description of the energies of the single-particle states and the sizes of the shell gaps have been analyzed. Relatively small sizes of the shell gaps in the SHN imply that these uncertainties can have a profound effect on the reliability of the predictions. In such a situation, other effects (such as softness of potential energy surface) have to be taken into account in analyzing the shell structure of SHN. The differences in the predictions of the fission barriers of superheavy nuclei in different theoretical frameworks have been discussed. Finally, the accuracy of the description of rotational properties of actinides and superheavy nuclei and the possibility of their use for configuration assignment in odd-mass light superheavy nuclei have been analyzed.

This material is based upon work supported by the U.S. Department of Energy, Office of Science, Office of Nuclear Physics under Award Numbers DE-FG02-07ER41459 and DE-SC0013037.

REFERENCES

[1] A. Sobiczewski, K. Pomorski, *Prog. Part. Nucl. Phys.* **58**, 292 (2007).
[2] R.D. Herzberg, P.T. Greenlees, *Prog. Part. Nucl. Phys.* **61**, 674 (2008).
[3] D. Vretenar, A.V. Afanasjev, G.A. Lalazissis, P. Ring, *Phys. Rep.* **409**, 101 (2005).
[4] A.V. Afanasjev *et al.*, *Phys. Rev.* **C67**, 024309 (2003).
[5] M. Bender *et al.*, *Phys. Rev.* **C60**, 034304 (1999).

[6] J.J. Li, W.H. Long, J. Margueron, N.V. Giai, *Phys. Lett.* **B732**, 169 (2014).
[7] S.E. Agbemava, A.V. Afanasjev, D. Ray, P. Ring, *Phys. Rev.* **C89**, 054320 (2014).
[8] A.V. Afanasjev, S. Frauendorf, *Phys. Rev.* **C71**, 024308 (2005).
[9] E.V. Litvinova, A.V. Afanasjev, *Phys. Rev.* **C84**, 014305 (2011).
[10] A.V. Afanasjev, E. Litvinova, `arXiv:1409.4855 [nucl-th]`.
[11] G.A. Lalazissis *et al.*, *Phys. Lett.* **B671**, 36 (2009).
[12] E. Litvinova, *Phys. Rev.* **C85**, 021303 (2012).
[13] A.V. Afanasjev, S. Shawaqfeh, *Phys. Lett.* **B706**, 177 (2011).
[14] M. Wang *et al.*, *Chin. Phys.* **C36**, (2012).
[15] T. Nikšić, D. Vretenar, P. Ring, *Phys. Rev.* **C78**, 034318 (2008).
[16] M. Bender, P.-H. Heenen, P.-G. Reinhard, *Rev. Mod. Phys.* **75**, 121 (2003).
[17] K. Rutz *et al.*, *Phys. Rev.* **C56**, 238 (1997).
[18] H. Abusara, A.V. Afanasjev, P. Ring, *Phys. Rev.* **C85**, 024314 (2012).
[19] A.V. Afanasjev, H. Abusara, P. Ring, *Eur. Phys. J. Web. Conf.* **62**, 03003 (2013).
[20] P. Möller, J. Nix, *Nucl. Phys. A* **536**, 20 (1992).
[21] A.V. Afanasjev, O. Abdurazakov, *Phys. Rev.* **C88**, 014320 (2013).
[22] S. Karatzikos, A.V. Afanasjev, G.A. Lalazissis, P. Ring, *Phys. Lett.* **B689**, 72 (2010).
[23] A. Baran *et al.*, *Phys. Rev.* **C84**, 054321 (2011).
[24] J. Sadhukhan *et al.*, *Phys. Rev.* **C88**, 064314 (2013).
[25] R. Rodríguez-Guzmán, L.M. Robledo, *Phys. Rev.* **C89**, 054310 (2014).
[26] P. Möller *et al.*, *Phys. Rev.* **C79**, 064304 (2009).
[27] M. Kowal, P. Jachimowicz. A. Sobiczewski, *Phys. Rev.* **C82**, 014303 (2010).
[28] A. Staszczak, A. Baran, W. Nazarewicz, *Phys. Rev.* **C87**, 024320 (2013).
[29] S. Hota, Ph.D. Thesis, University of Massachusset, Lowell 2012.
[30] A.V. Afanasjev, *Phys. Scr.* **89**, 054001 (2014).
[31] A.V. Afanasjev, P. Ring, J. König, *Nucl. Phys.* **A676**, 196 (2000).
[32] Z.-H. Zhang *et al.*, *Phys. Rev.* **C85**, 014324 (2012).
[33] X. Wang *et al.*, *Phys. Rev. Lett.* **102**, 122501 (2009).
[34] K. Abu Saleem *et al.*, *Phys. Rev.* **C70**, 024310 (2004).
[35] J.L. Egido, H.J. Mang, P. Ring, *Nucl. Phys.* **A334**, 1 (1980).
[36] P. Ring, P. Schuck, *The Nuclear Many-Body Problem*, Springer-Verlag, Berlin 1980.